On the Evaluation of Direct Laser Deposition of SS304L-SiC Composite: Layer Formation and Microstructure

Hassan A Sabour[1*], Mohammed A[1], Taha[2], Khaled Abdelghany[2], Ahmed F[2]. Youssef[2]

INTRODUCTION

Direct Laser Deposition (DLD) is defined as "an Additive Manufacturing process in which the laser energy is used to fuse powder material and deposit it on the substrate surface. It has different synonyms: Direct Light Fabrication, Direct Energy Deposition, Laser Rapid Forming, Direct Laser Fabrication, and Laser Solid Forming [1]. Besides producing and repairing 3D metal parts applications, the recent interest of researchers of DLD is the strengthening of raw material by adding hard ceramic particles powder. The high strength and corrosion resistance of stainless steel enables a wide range of industrial applications, whereas its lower hardness and wear properties limited its usage in high-temperature applications. To improve the mechanical properties, recently researchers evaluate adding ceramics particles to stainless steel such as Cr3C2, SiC, and WC. SiC characterized by the high resistance of creep and corrosion at high temperatures and achieves a good metallurgical bonding with stainless steel [2-7]. The laser surface alloying of SiC paste on vacuum sintered substrates of austenitic, ferritic, and duplex stainless steels using high power diode at constant scanning rates were done. It is stated that the processing parameters; scan speed and laser power, have great effects on the dissolution of SiC and resultant microstructure. The alloyed surface layer has a fine dendritic structure with iron-chromium carbide precipitations. The partial dissolution of SiC was noticed with the formation of Cr_7C_3 and iron silicides; FeSi and Fe_3Si. Due to surface modification, the highest hardening was 600 HV for laser alloying of SiC powder on duplex stainless steel [8]. The laser deposition of 316L stainless steel and its composites of 5 and 20 wt.% SiC using a high-power diode laser was done. The resultant microstructure was a fine grain stainless steel matrix with the formation of chromium carbide (Cr_3C_2) and Fe_2Si due to partial dissolution of SiC. The recommended optimum conditions were 700 W of laser power, 7.5 mm.s-1 of scan speed, and 60 mg.s-1 of powder feed rate. The hardness measurements recorded an increase in the deposited layer hardness from 150 HV of 316L stainless steel to 340 and 800 HV as add 5 and 20 wt.% SiC, respectively [9]. Direct laser deposition of 254 austenitic stainless steel composite of 20 wt.% SiC on mild steel substrate using 2 kW carbon dioxide laser, was investigated. Uniform and cracks free deposited layers were formed with low dilution. The microstructure was fine austenite dendrites surrounded by carbide; M_7C_3 eutectic mixture and all the incorporated SiC were dissolved. The improvement in hardness is from 240 HV to 966 HV as add 20 wt.% SiC [10]. This research study the influences of add SiC powder to stainless steel SS304L powder on track formation, defects, microstructure, and mechanical properties. The minimum laser power required to deposit complete tracks is theoretically calculated and compared with the experimental results.

EXPERIMENTAL WORK

Materials and Equipment

The deposited powders are SS304L (11Ni, 18Cr) and SiC (30C, 70Si) (Maker: Höganäs, Sweden). Their particle sizes are less than 125 μm. The substrate materials are plated 100x100 x10mm of mild steel (0.11C). The laser equipment is Nd: YAG DY 022 with a max power of 2.2 kW (Maker: ROFIN, Germany). The powder feeder is Sulzer 120A, (Maker: Sulzer Metco). The deposition head is YC50 with coaxial powder feeding (Maker: Precitec, Germany), Figure 1. Reichert stereomicroscopic X10 is used to inspect the surface feature. Olympic PME metallurgical microscope equipped with Panasonic digital camera and JOEL JSM5200 scanning electron microscope equipped by EDX analyzer is used for microstructure and phases investigations.

Figure 1: The coaxial nozzle YC50.
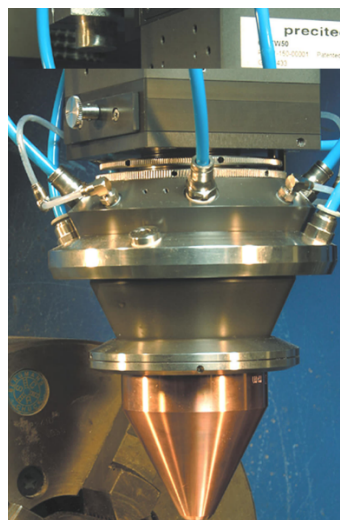
Procedure

SS304L powder was mixed with SiC powder at wt.% of 5, 10, and 15 using a VH powder mixer for 1 hour. The substrate sheets were cleaned using ultrasonic cleaner apparatus. The deposition head was mounted on a robot that was programmed to form multiple tracking lines with a length of 40 mm and adequate overlap. Experiments run while applying different values of laser power 200 to 1000W and moving speed from 25 to 100 cm min-1. Laser beam focus diameter was constant at 3 mm and powder feed rate was

[1]Central metallurgical research and development institute (CMRDI), Rapid Prototyping Lab, Elfelezat Street, Eltebbin, 12422, Helwan, Cairo, Egypt

[2]Ain-Sham University (ASU), Faculty of engineering, 1 El-Sarayat Street, Abbassia, 11517, Cairo, Egypt

*Corresponding to: Sabour HA, Central metallurgical research and development institute CMRDI, Rapid Prototyping Lab. 1 Elfelezat Street, Eltebbin, 12422, Helwan, Cairo, Egypt; Tel: 00201144942651; E-mail: helkordy3000@yahoo.com

constant at 8 g min-1. After, all specimens were cleaned and polished by 320-1000 sandpaper. For metallographic examination, samples are polished by 320, 400, 600, 800, and 1000 sandpaper and etched by 40 ml HNO3, 10 ml HF, and 40 ml H2O for 5-10 sec. The microhardness measurements are carried out at an applied load of 200 g with a loading time of 15 sec.

RESULTS AND DISCUSSIONS

Complete Layer Deposition

The effect of processing parameters on the formation of deposited tracks was investigated and illustrated. The macrographs of deposited SS304L powder on mild steel substrate at scan speed range from 50 to 100 cm.min-1 and laser power range from 400 to 800 W, is shown in Figure 2. Below laser power 400 W, there is no deposition of SS powder. The laser power was insufficient to melt the surface of the substrate or the powder particles. The layer formation stages from no deposition to complete overlapping layer were as following:

- At laser power 400 W and scanning speed 100 cm.min-1: only a small amount of powder stacked on the substrate surface,
- At laser power 400 W and scanning speed 75 cm.min-1: the deposited powder agglomerated and formed detached tracks. The laser power was enough to melt the top substrate and some of the powder.
- At laser power 400 W and scanning speed 50 cm.min-1: thin connected tracks appeared. The deposited layer consists of several tracks stacked side by side with spacing between them called track spacing.
- At laser power 600 W and scanning speed 100 cm.min-1: powder stacked on the substrate.
- At laser power 600 W and scanning speed 75 cm.min-1: thin connected tracks were formed.
- At laser power 600 W and scanning speed 50 cm.min-1; wider tracks were formed.
- At laser power of 800, overlapped tracks appeared at different scan speeds and the track width increased while decreasing the scan speed,

Figure 2: Series of deposited layer surface shapes of SS304L at different scan speeds and laser powers.
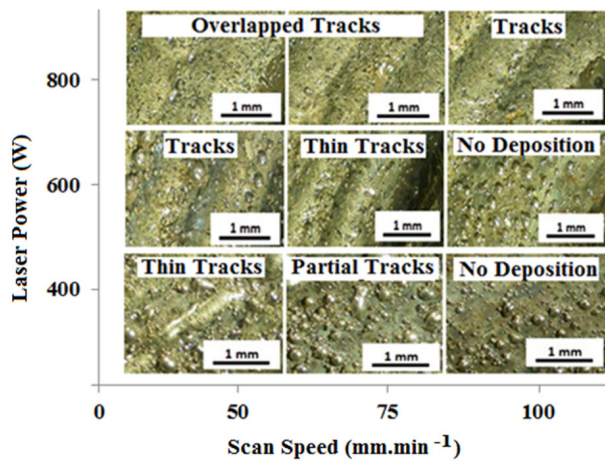
A series of optical micrographs of deposited SS304L composite with 10 wt.% SiCp on mild steel substrate at scan speed from 50 to 100 cm.min-1 and laser power from 400 to 800 w, is illustrated in Figure 3. The formation stages of the complete deposited layer for 10 wt.% SiC composite are similar to SS304L. The difference is that the starting point of forming thin and connected tracks for composites is at a lower scan speed than SS304L. In composite, the thin tracks formed at laser power 400 and scan speed 75 cm.min-1 or at laser power 600 and scan speed 100 cm.min-1. It is attributed to that the laser radiation absorption of SiC powder is larger than the laser radiation absorption of Fe powder, leading to an increase in the effective laser energy delivered to the substrate surface. Therefore lower laser power or higher scan speed is enough to form thin tracks in

composites of SiC. It can be noticed that the composite with SiC powder formed darker color of deposited tracks than those of SS304L. It is due to carbon burning after the partial dissolution of SiC powder to C and Si. The dark color of deposited tracks can be removed by cleaning methods. The effect of laser power on the formation stages of deposited tracks for SS304L powder and its composites with SiC, can be summarized in Figure 4. Also the tracks width of SS304L and its composites with 5, 10 and 15wt.% SiC at scan speed 75cm.min-1 and different laser power, are shown in Figure 4. The track width increased as increasing the laser power at constant scan speed. It is due to increasing the applied laser energy on the deposited powder leading to an increase in the deposition rate and track width. The track width of composites recorded higher values than SS304L and increased as increasing the percentage of add SiC powder.

Figure 3: Series of deposited layer surface shapes of SS304L+10 wt.% SiC at different scan speeds and laser powers.
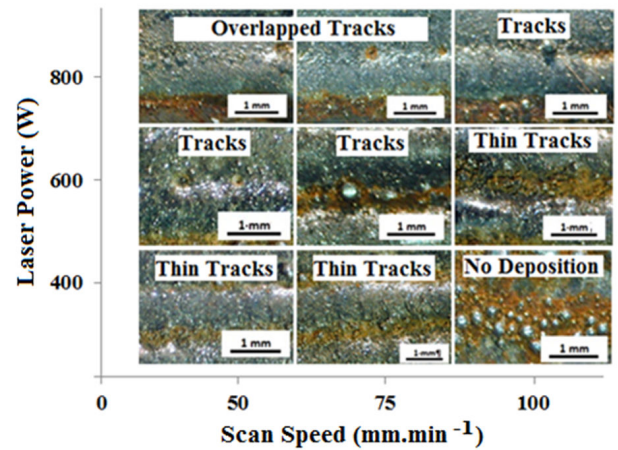
Figure 4: Effect of laser power on layer formation stages and track width of SS304L at scan speed 75 cm.min-1
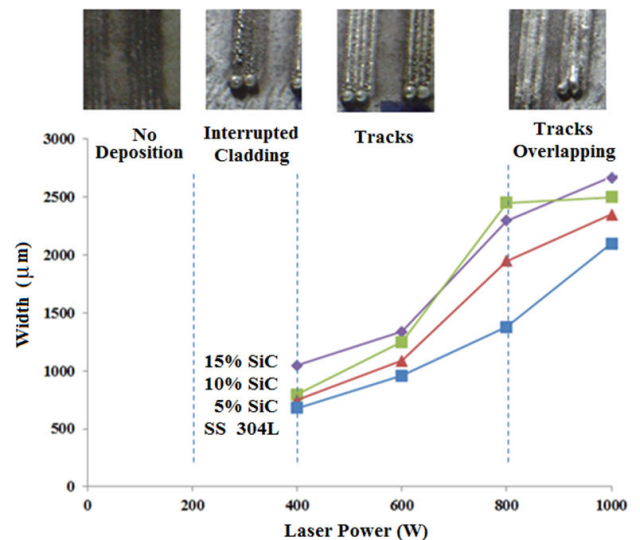
The required laser energy to deposit deposited tracks, Pmin; In case of using metal-ceramic powder mixture for deposition, ceramic particles are not melted, but only heated due to laser beam propagating through the powder cloud. The focused laser beam melts the surface of the target material and generates a small molten pool of base material, while powder delivered into this same spot is absorbed into the melt pool, thus generating a thin deposit. The transmitted laser power is absorbed by the substrate according to its absorption coefficient. Wei et al, who modeled the heat source to simulate laser deposition, reported that the laser beam propagates through the powder cloud, where the attenuated laser power is absorbed according to the powder absorption coefficient while the rest is reflected out of the

process zone [11-12]. The total absorbed energy includes the transmitted by the substrate and the laser power absorbed by the powder. The absorbed laser energy depends on laser properties (wavelength, polarization, angle of incidence (intensity, non-linear effects) and metal properties (chemical composition, temperature, roughness topography, oxide layers, contamination (dust, dirt, surface and bulk, defects, etc) [13-15]. The amount of laser energy absorbed by the substrate determines the temperature within the substrate. It is needed to melt the substrate surface and generates a small molten pool of base material, while powder delivered into this same spot is absorbed into the melt pool, thus generating a thin deposit. The minimum laser power, Pmin, required to melt both substrates and deposited powder and form solid metallic bonding between the coating and substrate material can be estimated based on the absorption coefficients and related physical properties. Adding the power absorbed by each of mild steel substrate surfaces and both SS304L and SiCp powder powders, Equation 1, can be used to calculate Pmin [11]:

$$\gamma \times P_{min} = 0.5 \times \lambda_s \times (T_{ms} - T_0) \times \left(\frac{\pi}{\alpha_s \times t_{in}}\right)^{0.5} + \eta \times M^{\cdot} \times \left(L_c + (C_{pc} \times T_{mc})\right) \quad (1)$$

On the other hand, Pmin can be estimated when the layer geometry is specified. For this purpose, a typical cross-section of a full track bonded with the mild steel substrate, obtained in the present experiments. This is similar to that of previous research on different laser deposited layers. Defining the geometrical features and knowing the physical data of both substrate and deposited powder, Pmin can be calculated similarly to previous work by Equation 2 [11]:

$$\gamma \times P_{min} = A_{mix} \times \rho_s \times v \left(L_s + (C_{ps} \times T_{ms})\right) + A_c \times \rho_c \times v \left(L_c + (C_{pc} \times T_{mc})\right) \quad (2)$$

Where,

γ is the absorption coefficient of powder, λs is the thermal conductivity of substrate,

Tms is melting temperature of substrate, To is initial temperature of substrate,

αs is thermal diffusivity of substrate, tin, sec, is an interaction time,

d is the focus diameter of laser beam, v mm.sec-1, is scan speed,

η is the powder catchment efficiency, M´ is the powder feed rate (0.13 gm.sec-1)

Lc is latent heat of powder   Cpc is heat capacity of powder

Tmc is melting temperature of powder Amix is the dilution area

ρs is the density of the substrate Ls is latent heat of substrate

Cps is heat capacity of substrate Tms is melting temperature of substrate

Ac is the area of a deposited track. ρc is the density of the coating material.

Data available in the literature on the absorption coefficient γ of each substrate and powder materials greatly differ. For a cleaned surface of the mild steel substrate, an absorption coefficient γ of 0.4, which sharply increases at the melting temperature, was reported. In another work, a value of γ of 0.7 has been reported for mild steel surfaces with a roughness of 4.5μm. This value is selected in this work where the mild steel surface was prepared using grinding paper grit 180. For a SS 316 powder, previous work reported absorption coefficient γ values ranging between 0.3 and 0.75, while for SiCp, a value of 6.63 was reported. Based on the above, in this work, the value of γ is taken constantly as 0.7 [12-15].

Power received by the substrate material is reached at the end of an interaction time, tin , which depends on the applied scan speed v and the focus diameter of laser beam d, (constant =3mm).

tin, sec., is the interaction time at which the power received by the substrate material is reached. tin can be computed as d/v, thus it depends on the applied scan speed v (mm.sec-1) and the focus diameter of laser beam d, mm (= 3mm). The Calculated varied with applied v of 4.17, 8.33, 12.5, and 16.67 mm/sec as 0.728, 0.361, 0.24 and 0.18 sec, respectively.

η, is the powder catchment efficiency which determines the amount of injected powder that remains into the melt pool to form the track and can

be simply calculated as η = Amp/Apj. Where Amp is the melt pool area and Apj is the area of the powder jet when it reaches the melt pool. Similar to previous work, which also involved losses in the feeding system, a value for η of 0.85 is considered due to the design of the powder delivery system and coaxial nozzle.

Calculated Pmin as a function of applied v, by using Equation 1 and Equation 2, shows a linear relationship with increasing v from 4.17 to 16.67 mm s-1, Figure 5. The plotting of applied laser power and scanning speeds in the present work versus the points of calculated Pmin from Equation 1 & 2, shows no track deposition is found, for points below the straight-line of minimum laser power, Figure 5. Comparing the applied laser power at different scanning speed with the calculated required power for deposition based on physical properties and geometrical dimensions of the specimens, it indicates close agreement.

Figure 5: Experimental work via the calculated Pmin using the geometry of tracks and physical properties of powder and substrate.
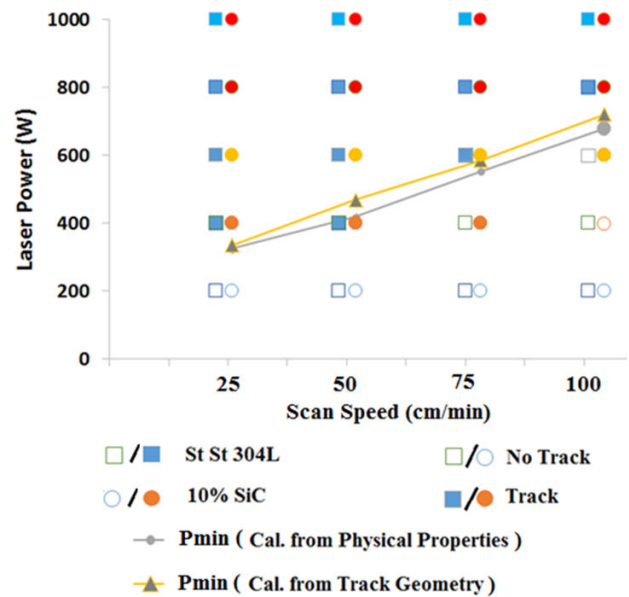
Track Porosity

Macroscopic and microscopic images revealed two types of pores; namely gas pores and inter-run pores, which consider as a common defect in the direct laser deposition technique. Such defects have been also observed by previous researchers, who reported that it could be minimized or avoided by processing parameters optimization.

Gas Porosity; deposited track cross-sectional photomicrographs show fine and coarse gas pores, which is observed in both cases of SS304L and its composites with SiC. The recent research stated that pores up to 50 microns are fine pores, while the courser ones are up to 300 microns [10-13]. A sample of fine and coarse pores in 15 wt.% of SiC composite with SS304L, produced at a laser power of 400 W and a scan speed of 50 cm/min, is indicated in Figure 6. The generation of gas pores is due to gas entrapped after rapid solidification of the molten pool [16]. By adding SiC powder, fumes are formed after burning free carbon during laser processing, thus leading to an increase of gas entrapped in the molten pool. This happens in the present work, although that the deposited powders have been thermally roasted before the deposited experiment. Coarser pores are possibly due to fine and un-melted powder particles injected into the molten pool where the melt pool may trap the shielding or carrier gas leading to porosity during rapid solidification. The percentage of porosities are plotted for SS304L and its composites with [5, 10, and 15] wt.% SiC at constant scan speed and different laser powers, Figure 7. It can be seen that the total volume fraction of porosity generally decreases with increasing laser power. This is remarkable in the case of SiC composites powder, which includes larger and smaller pores and thus much more porosity level compared to SS304L powder as a result of increasing the percentages of free

carbon in the molten material. Increasing laser power results in increasing solidification time leading to minimize the gas entrapped and so on decreasing the gas pores. In the present work, the smallest pore's percentage of 0.23% in the case of SS304L deposited powder is obtained at a larger laser power of 1000 W, which is evidence of the ability to produce fully dense products by the laser deposition technique.

Inter-run Pores; The cross-sections of the deposited layer for SS304L, produced at scan speed 50 cm/min and different laser power, are presented in Figure 8. As shown in the figure, the inter-run pores obviously appeared in the area between overlapping tracks. Such behaviour is due to the lack of powder fusion as a result of decreasing the effective delivered laser energy (low laser power or high scan speed) leading to prevent melting of all powder particles, especially at the overlapping area. As increasing of laser power to 800 W, the inter-run pores disappeared. Further increase of laser power leads to an increase in the inter-run pores. It is attributed to enlarge the mixing area and increase the dilution percentage, leading to more turbulent of the molten pool, which affects the appearance of inter-run pores. The add wt.% SiC to SS304L powder increases the inter-run pores due to increasing the percentages of fumes that attenuate the laser beam leading to a lack of fusion. Generally, to prevent the formation of layer defects, laser power should be carefully increased, while the percentage of added wt.% SiC should be decreased.

Figure 6: Observed fine and coarse pores in deposited track of SS304L with 15 wt. % SiC at laser power of 1000 W and scan speed 25 cm.min-1.
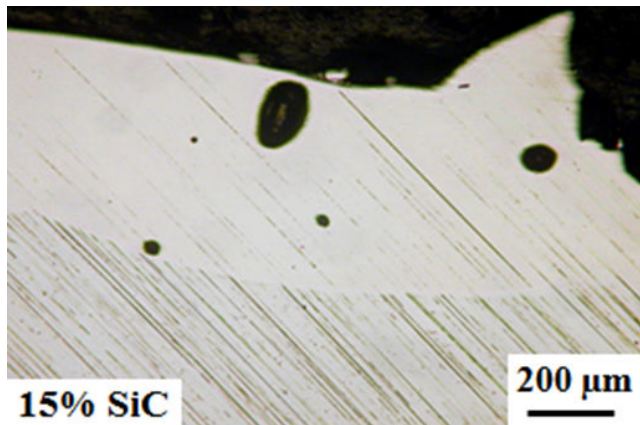
Figure 7: The vol. % of pores for SS304L and its composites of 5, 10 and 15 wt. % SiC at scan speed 50 cm.min-1 and different laser powers.
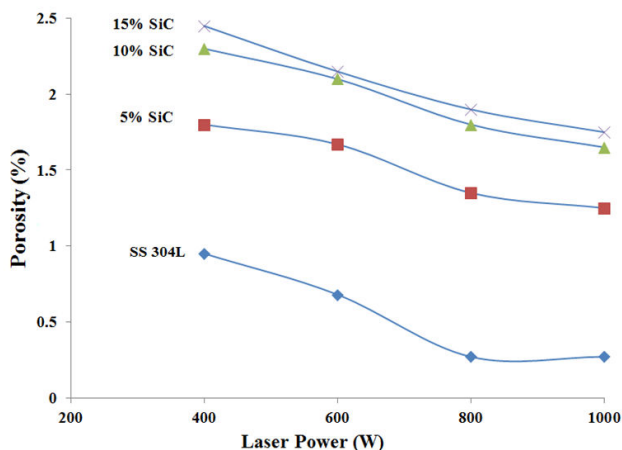
Figure 8: Inter-run pores in deposited layers of SS304L at scan speed of 50 cm.min-1 and different laser power.

a. Laser Power = 600W

b. Laser Power = 800W

c. Laser Power = 1000W
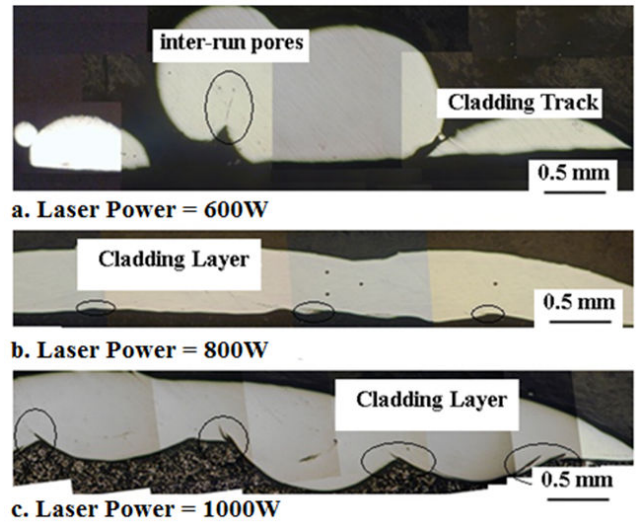
Track Microstructure

The deposited track contains mainly three areas; track area, mixing area, and heat-affected zone (HAZ) area, which is presented in a schematic drawing, Figure 9. The structures of such areas are influenced by laser heating and the solidification of the melting pool. The single-track cross-sectional macrostructure of SS304L, produced at a laser power of 400 and scan speed of 50, is shown in Figure 10. Over the HAZ area, the interface line can be seen obviously, which is free from cracks. Beyond that, the epitaxial growth starts on heterogeneous sites of the interface line, which is due to differences in the structure of the substrate and the deposited track. Different dendritic structure features are noticed from the interface line to the top surface of the track area. In the top surface of the deposited track at zone A, a fine dendritic structure is noticed, which is formed due to high cooling rates of laser deposition, while the structure is lamellar dendritic in the middle of the track at zone B and coarse dendritic in the mixing area, Figure 10 b-c. It is attributed to the variety in temperature distribution, temperature gradient, and solidification velocity leading to varying in the cooling rate of different zones and different structures formed [15]. The shape of the track dendritic structure is influenced by applied laser power. The effect of laser power on the dendritic structure of SS304L at different laser power is shown in Figure 11. As shown in the figure, the increasing of laser power leads to coarsening the dendrite structure. It is attributed to reducing of cooling rate and increasing the solidification time leading to form the course structure. The microstructure phase analysis of single track SS304L showed only austenite phase; γ as a strong peak, while different phases appear beside γ-phase in composites of SiC such as SiC, Cr_7C_3, Fe_2Si, and martensite phases, Figure 12. The formation of SiC phase is evidence of partial dissolution of SiC powder, which is also revealed by metallographic examination, Figure 13. Similar results are observed by previous studies, which mention that the remained SiC forms metal matrix composite (MMC) with stainless steel matrix [17]. The temperature of the melting pool is increased over to the melting temperature of SiC powder during laser deposition leading to dissolving the SiC into Si and C. Beyond that the stainless steel is super-saturated by free Si leading to form Fe_2Si precipitation. The formation of Cr_7C_3 precipitation is due to the presence of carbide former and free carbon which encourages the formation of carbide [18]. A few peaks of martensite are observed at composites of SiC due to the high cooling rate with more free carbon in the matrix.

Figure 9: Schematic representation of deposited track.
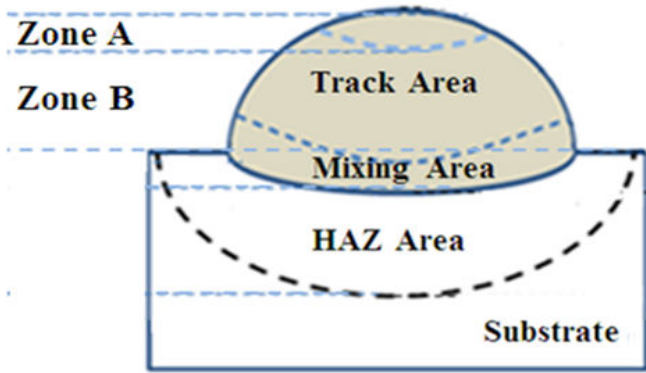
Figure 10: Cross sectional macrostructure single track of SS304L at laser power 400 W and scan speed 50 cm.min-1, a) single track, b) zone A, c) zone b, d) mixing area.

a. Single Track

b. Zone A

c. Zone B

d. Mixing Area
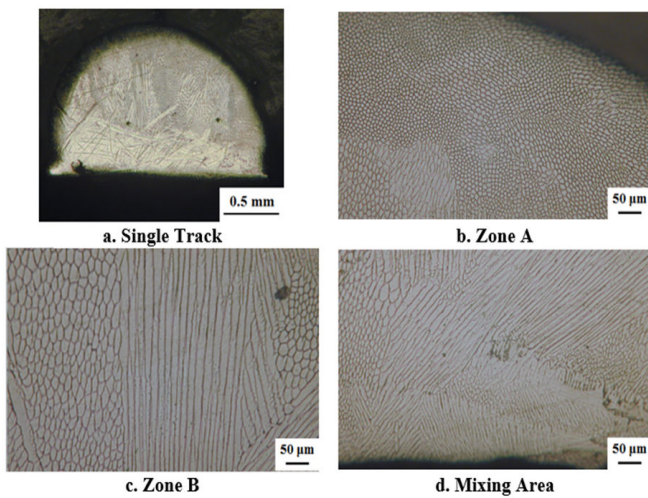
Figure 11: Cross sectional microstructure for SS304L at scan speed 50 cm.min-1 a) laser power 800 W, b) laser power 1000 W.

a. Laser Power 800 W

b. Laser power 1000 W
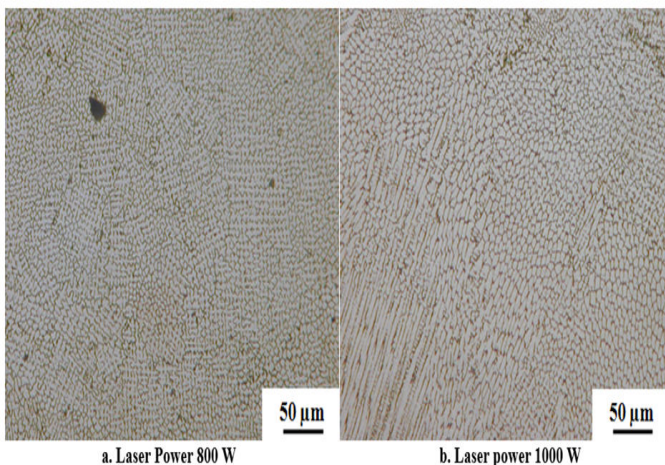
Figure 12: XRD analysis for SS304L and its composite of 10 wt.% SiC at laser power 400 W and scan speed of 50 cm.min-1.
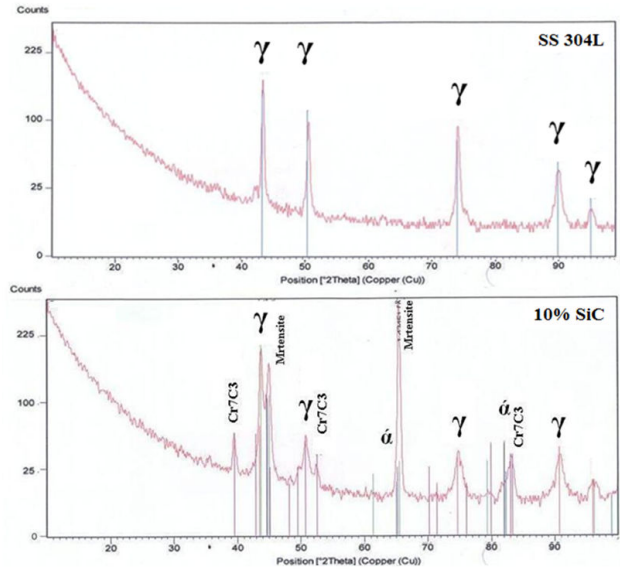
Figure 13: Cross sectional microstructure of 10 wt.% SiC at laser power 400 W and scan speed of 50 cm.min-1.
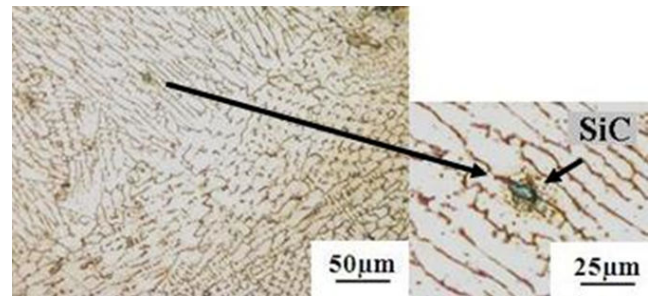
Hardness Measurements

The microhardness measurements in the track area for SS304L and its composites of [5, 10, and 15] wt.% SiC at a scan speed of 50 cm.min-1 and different laser power, are shown in Figure 14. The composites of [5, 10, and 15] wt.% SiC recorded higher hardness measurements than SS304L. The increase in hardness measurement is due to combining effects of different hardening mechanisms such as dispersion hardening, microstructural refinement, and solid solution strengthening [17]. The hardness of composites increases as increasing the wt.% of SiC, which is due to the role of remained SiC and precipitations in changing of measured hardness [18]. The influence of laser power on the microhardness of deposited tracks for SS and its composites is presented in Figure 14. The increasing As increasing laser power, the hardness is slightly decreased for both alloy and composites, which is due to microstructure coarsening as increasing laser power. Moreover in composites, the decreasing of hardness is due to a decrease in the remained SiC particles (higher hardness compounds) and increases the precipitations of silicide and carbides (lower hardness compounds) as increasing laser power.

Figure 14: The hardness measurements in track area for SS304L and its composites of 5, 10 and 15 wt.% SiC at scan speed of 25 cm.min-1 and differant laser power.
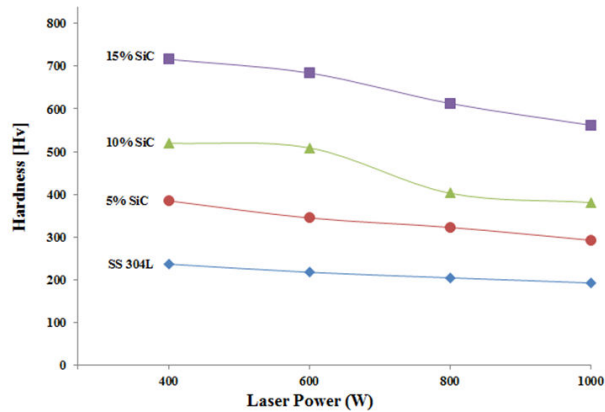
CONCLUSIONS

Direct laser deposition of SS304L and its composites with SiC powder represents results in good quality deposited tracks. Comparing the applied laser power at different scanning speeds with the theoretically calculated laser power required for melting and deposition - based on physical properties and geometrical dimensions of the specimens - indicated close agreement. The laser power controls track formation and defects. The formation of a completely deposited layer passes through different stages, from no deposition to overlapping tracks, depending on the processing parameters. The total volume fraction of porosity decreases with increasing the laser power. The smallest pore percentage is 0.23% in the case of SS304L and high laser power of 1000 W, which is evidence of the ability to produce fully dense products by the direct laser deposition technique. The microstructure of SS304L composites with SiC is in form of a combined composite microstructure. The first is MMC of remained SiC particles in a matrix of austenitic stainless steel dendritic structure, and the second is In-Situ composite due to the partial dissolution of SiC particles and the formation of Cr_7C_3 & Fe_2Si precipitations. The adding SiC to SS304L reflected to improve in hardness measurements.

REFERENCES

1. Lin C , Suiyuan Ch, Mingwei W, et al, Study of surface topography detection and analysis methods of direct laser deposition 24CrNiMo alloy steel, Optics and Laser Technology, 2021, 135,106661

2. Rashkovets M, Mazzarisi M, Nikulina A, Casalino G, Analysis of laser direct stainless steel powder deposition on Ti6Al4V substrate, Materials Letters, 2020, 274, 128064

3. Jichang X, Zhaozhen H, Haifei L, Buyun Z, Xiang X, Jianbo L, Additive manufacturing of tantalum-zirconium alloy coating for corrosion and wear application by laser directed energy deposition on Ti6Al4V, Surface & Coatings Technology, 2021, 411, 127006

4. Reda S, Hussein A, Nofal A, Ibrahim S, Elgazzar H, Sabour H, Material, 2017, 10, 1178.

5. Pouya S, Mohamed T, Brendan O, Richard J, Xing Z, Yiliang L, Enhancing hypervelocity impact resistance of titanium substrate using Ti/SiC Metal Matrix, Nanocomposite coating Composites, 2020,194, 108068

6. Guifang S, Sudip B, Guru P, Ashish D, Mazumder J, Microstructure evolution during laser-aided direct metal deposition of alloy tool steel, Scripta Materialia, 2011, 64, 454-457

7. Taha M, Yousef A, Gany K, Sabour H, On selective laser melting of Ultra High Carbon Steel: Effect of scan speed and post heat treatment, Materialwissenschaft Und Werkstofftechnik, 2012

8. Brytan Z, Dobrzański L, Pakieła W, Laser surface alloying of sintered stainless steels with SiC powder, 2011, 47,

9. Abbas G, Ghazanfar U, Wear, 2005, 258, 258

10. Majumdar D, Li L, Metals and Materials Society, 2009.

11. Wei Y, Laser Materials Interactions During Cladding, Faculty of Engineering Technology, University of Twente, the Netherlands, 2015

12. Wei Y, Pathiraja B, 2D modelling of clad geometry and resulting thermal cycles during laser cladding, Journal of Materials Processing Technology, 2016, 230, 217–232

13. Zaitsev A, Ermolaev G, Polyanskiy T,. Gurin A, Study of absorption coefficient in laser cutting of metal, AIP Conference Proceedings, 2018, 2027, 030109

14. Florian W, Daniel E, Konard W, Absorptivity measurements and heat source modelling to simulate laser cladding, Physics Procedia, 2016, 83, 1424 – 1434

15. Johannes T, Alexander M, Gabe G, Matthews J, In situ absorptivity measurements of metallic powders during laser powder-bedfusion additive manufacturing, Applied Materials Today, 2017, 9, 341–349

16. Chunyang Z, Shusen Z, Yibo W, Falan L, Wenyan G, Xuechun L, Mitigation of pores generation at overlapping zone during laser cladding, Journal of Materials Processing Technology, 2015, 216, 369–374

17. Dutta M, Lin L, Studies on Direct Laser of SiC Dispersed AISI 316L Stainless Steel, Metallurgical and Materials Transactions, 2009, 40a

18. Dutta M, Ajeet K, Lin L, Direct laser cladding of SiC dispersed AISI316L stainless steel, Tribology International, 2008 .